JOURNAL OF SOLID STATE CHEMISTRY 59, 103–110 (1985)

Crystal Structure of $Ba_6Zn_7F_{26}$

J. RENAUDIN, M. SAMOUËL,* M. LEBLANC, A. DE KOZAK,* AND G. FEREY

*Laboratoire des Fluorures et Oxyfluorures Ioniques, UA CNRS 449, Faculté des Sciences, Université du Maine, Route de Laval, 72017 Le Mans Cédex, and *Laboratoire de Chimie Minérale, ER CNRS 9, Université P. et M. Curie, Tour 54, 4 place Jussieu, 75230 Paris Cédex 05, France*

Received October 19, 1984; in revised form January 17, 1985

$Ba_6Zn_7F_{26}$ is monoclinic (S.G. $C2/m$): $a = 19.46(1)$ Å, $b = 5.956(2)$ Å, $c = 12.243(5)$ Å, $\beta = 128.88(1)°$, $Z = 2$. The structure has been refined from 1730 independent reflections to $R = 0.046$ ($R_\omega = 0.049$). The three dimensional network can be described as layers containing intergrown rutile and perovskite units. Two layers are connected by isolated octahedra. An alternative description uses defective rutile blocks joined by isolated octahedra. The comparison with the $Ba_2Ni_3F_{10}$ structure suggests a "condensation" mechanism which could explain the progressive transformation from perovskite related structures to the rutile structure. All the Ba^{2+} (three (4*i*) sites), form a dense packing with F^-. They are dodeca-coordinated, with the hcp and fcc type for Ba_3 and (Ba_1/Ba_2), respectively.

Introduction

In the binary systems BaF_2–MF_2 (M = Co, Ni, Cu, Zn (*1*)), many compounds appear for a molar ratio M/Ba > 1. Starting from the composition $BaMF_4$ whose bidimensional structure is well known (*2*, *3*), the increase of the M/Ba ratio successively leads to $Ba_6M_7F_{26}$ (M = Cu, Zn), $Ba_2M_3F_{10}$ (M = Zn (*4*), Co, Ni), and $Ba_2M_7F_{18}$ (M = Ni, Cu, Zn). After the structural determination of $Ba_2Ni_3F_{10}$ that we performed some years ago (*5*), we are now investigating the crystal structure of the other compounds. This paper is devoted to $Ba_6Zn_7F_{26}$, which was previously formulated $Ba_5Zn_6F_{22}$ (*1*). Its structure will be compared with $Ba_2Ni_3F_{10}$ in order to show the progressive intergrowth of perovskite and rutile blocks when M/Ba increases.

Experimental

Transparent platelets of $Ba_6Zn_7F_{26}$ are grown either by hydrothermal synthesis in 49% HF [BaF_2] = 6 *M*, [MF_2] = 7 *M* at 400°C, 205 MPa for 3 days according to a method previously described (*6*) or by long heating (750°C—2 weeks) of a stoichiometric mixture of the corresponding fluorides in sealed platinum tubes. (100) planes correspond to the largest dimensions of the platelets (Table I).

Despite an orthorhombic pseudosymmetry, Laue and precession photographs show that the true symmetry of the crystals is monoclinic, with space group $C2/m$ (Table I). Intensity data were collected on a CAD 4 Nonius diffractometer. The experimental conditions of data collection are summarized in Table II. Corrections for

0022-4596/85 $3.00

Lorentz, polarization effects and for absorption are applied, using the SHELX program (*7*) for all calculations. Atomic scattering factors are taken from the "International Tables for X-Ray Crystallography" (*8*) for Ba^{2+}, Zn^{2+}, F^-.

Structure Determination

The structure has been solved from a Patterson map which allows us to localize the 12 barium ions of the cell in three 4*i* sites *x*0*z*. The refinement of the corresponding coordinates leads to a reliability factor of 0.421. A Fourier map then reveals the position of the Zn^{2+} ions (R = 0.135). The F^- ions are located from a new Fourier synthesis. The refinement of their atomic parameters and isotropic temperature factors easily converges to R = 0.064 (R_ω = 0.064). The residual falls to 0.046 (R_ω = 0.049) when applying anisotropic thermal motion for all atoms and a secondary extinction factor of 5.1 × 10^{-8}. A final difference Fourier map gives a maximum peak of 2.3 $e^-/Å^3$ corresponding to a position close to Ba2 ion. Refinements in the noncentric *C*2 and *Cm* space groups do not improve the results.

Table III presents the final results for the 16 independent positions; characteristic distances are listed in Tables IV and VII. The list of structure factors can be obtained on request to one of the authors (G.F.).

Discussion of the Structure

Figure 1 presents the (010) projection of $Ba_6Zn_7F_{26}$. Zinc ions occupy four kinds of crystallographic sites, and are all roughly hexacoordinated by F^- (Table IV). All the fluorine atoms of Zn(1) and Zn(4) octahedra are bridging ones. Zn(2) octahedra possess four terminal and two bridging F^-. The inverse situation occurs with Zn(3). It is noteworthy that there are two kinds of bridging fluorine ions in the structure: they can belong to two or three octahedra (Table V)

TABLE I

EXPERIMENTAL DATA FOR $Ba_6Zn_7F_{26}$ CRYSTALS

Symmetry: monoclinic	Cell parameters	a = 19.46(1) Å
Space group: $C2/m$ (no 12)		b = 5.956(2) Å
Conditions: $h + k = 2n$		c = 12.243(5) Å
ρ_{exp}: 5.23(11) g · cm^{-3}		β = 128.88(1)°
ρ_{calc} 5.32 g · cm^{-3}		V = 1104 Å^3
		Z = 2

TABLE II

CHARACTERISTICS OF DATA COLLECTION

Crystal dimensions: 0.07 × 0.07 × 0.025 mm^3		
Radiation: Mo$K\alpha$		
Linear absorption coefficient: 184 cm^{-1}		
Range measured:	$2° < \theta < 35°$	$-26 < h < 26$
	$-9 < k < 9$	$0 < l < 19$
Reflections measured:		
Total	3447	R = 0.046
Independent	1983	R_ω = 0.049
With $\lvert F\rvert/\sigma(\lvert F\rvert) > 6$	1730	
Secondary extinction: 5.1(4) × 10^{-8}		
Transmission factor maximum: 0.648; minimum: 0.310		
Operating features:		
Monochromator: graphite		
Scan mode: ω–2θ	sweep $S = (1.80 + 0.45tg2\theta)°$	
Scintillation counter aperture: 3.00 mm		
Scanning speed: $v = (20.1166/NV)° \cdot mn^{-1}$ with NV integer		

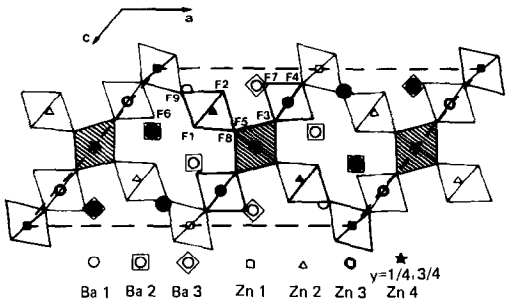

FIG. 1. (010) projection of $Ba_6Zn_7F_{26}$. Shaded octahedra correspond to the rutile chains which develop along [010]. The numbers refer to the type of fluorine atoms of Table III. Open symbols correspond to $y = 0$ and full symbols to $y = \frac{1}{2}$.

TABLE III

ATOMIC COORDINATES AND ANISOTROPIC THERMAL PARAMETERS OF $Ba_6Zn_7F_{26}$[a,b]

Atom	Site	x	y	z	U_{11}	U_{22}	U_{33}	U_{23}	U_{13}	U_{12}	B_{eq}
Ba1	4*i*	1475(1)	0	1522(1)	135(4)	94(3)	113(3)	0	84(3)	0	0,90
Ba2	4*i*	1433(1)	½	4043(1)	127(4)	166(4)	115(3)	0	84(3)	0	1,07
Ba3	4*i*	3437(1)	0	1054(1)	127(4)	115(3)	137(3)	0	86(3)	0	1,00
Zn1	2*b*	0	½	0	86(10)	55(8)	69(8)	0	44(8)	0	0,55
Zn2	4*i*	2786(1)	½	2879(2)	102(7)	76(6)	118(6)	0	75(6)	0	0,78
Zn3	4*i*	4877(1)	½	2215(2)	140(8)	98(6)	112(6)	0	87(7)	0	0,92
Zn4	4*h*	½	2445(3)	½	142(7)	70(6)	99(6)	0	76(6)	0	0,82
F1	8*j*	2586(4)	2640(10)	3809(6)	183(28)	104(24)	152(25)	27(20)	113(24)	−12(22)	1,15
F2	8*j*	2546(4)	2697(10)	1486(6)	171(31)	113(25)	175(28)	−28(20)	113(27)	− 6(21)	1,21
F3	8*j*	4910(5)	2349(10)	3254(6)	246(33)	112(25)	147(26)	5(20)	123(27)	−10(24)	1,33
F4	8*j*	4818(7)	2489(16)	0923(8)	564(67)	569(62)	181(35)	−78(35)	106(42)	348(52)	3,46
F5	4*i*	4102(6)	0	4200(10)	103(39)	86(34)	236(43)	0	87(37)	0	1,12
F6	4*i*	6153(8)	½	3278(12)	173(52)	701(87)	240(51)	0	144(47)	0	2,93
F7	4*i*	3599(7)	½	0809(10)	115(44)	446(61)	167(41)	0	86(38)	0	1,92
F8	4*i*	4128(6)	½	4204(9)	129(42)	85(35)	199(41)	0	73(37)	0	1,09
F9	4*i*	1290(7)	½	1563(11)	114(47)	372(61)	247(51)	0	10(42)	0	1,93

[a] All the values are × 10^4. Standard deviations are in parentheses.

[b] The vibrational coefficients are relative to the expression $T = \exp[-2\pi^2(h^2a^{*2}U_{11} + k^2b^{*2}U_{22} + l^2c^{*2}U_{33} + 2klb^*c^*U_{23} + 2hla^*c^*U_{13} + 2hka^*b^*U_{12})]$.

TABLE IV

INTERATOMIC DISTANCES (Å) AND BOND ANGLES (°) OF Zn OCTAHEDRA IN $Ba_6Zn_7F_{26}$

Zn1 Octahedron: Symmetry 2/*m*		
		Angle F–Zn–F
Zn1–F4[b]: 4 × 2.025(10)	F4–F4: 2 × 2.766	86.1(4)
Zn1–F9[b]: 2 × 1.983(11)	F4–F9: 4 × 2.801	88.6(3)
⟨Zn1–F⟩ 2.011	F4–F9: 4 × 2.872	91.5(3)
	F4–F4: 2 × 2.978	94.6(4)
Zn2 octahedron: Symmetry *m*		
Zn2–F1[f]: 2 × 1.994(6)	F1–F9: 2 × 2.686	77.5(3)
Zn2–F2[f]: 2 × 2.001(6)	F2–F2: 2.743	86.4(3)
Zn2–F8[b]: 2.031(10)	F1–F2: 2 × 2.795	88.8(3)
Zn2–F9[b]: 2.276(11)	F1–F1: 2.810	89.7(3)
⟨Zn2–F⟩ 2.049	F2–F9: 2 × 2.856	83.4(3)
	F1–F8: 2 × 3.064	99.2(3)
F8–Zn2–F9: 175.1(4)	F2–F8: 2 × 3.089	100.0(3)
Zn3 octahedron: Symmetry *m*		
Zn3–F7[f]: 1.942(10)	F4–F7: 2 × 2.721	84.2(3)
Zn3–F6[f]: 1.951(12)	F3–F4: 2 × 2.742	83.3(3)
Zn3–F3[b]: 2 × 2.004(6)	F4–F6: 2 × 2.814	87.0(3)
Zn3–F4[b]: 2 × 2.127(7)	F3–F6: 2 × 2.884	93.2(3)
⟨Zn3–F⟩ 2.025	F3–F7: 2 × 2.902	94.4(3)
	F4–F4 2.978	89.1(4)
F6–Zn3–F7: 167.7(4)	F3–F3: 3.158	104.0(3)
Zn4 octahedron: Symmetry 2		
Zn4–F5[b]: 2 × 1.996(6)	F8–F8: 2.651	82.0(4)
Zn4–F8[b]: 2 × 2.016(7)	F5–F5: 2.721	86.3(4)
Zn4–F3[b]: 2 × 2.032(7)	F3–F5: 2 × 2.799	88.0(3)
⟨Zn4–F⟩ 2.014	F3–F5: 2 × 2.832	89.3(3)
Zn4–F5–Zn4: 93.7(4)	F3–F8: 2 × 2.902	91.3(3)
Zn4–F8–Zn4: 92.5(4)	F3–F8: 2 × 2.903	
F3–Zn4–F3: 176.8(4)	F5–F8: 2 × 2.978	95.8(3)
Zn4–Zn4: 2.913(3)		
⟨Zn–F[f]⟩ 1.980 ⟨Zn–F[b]⟩ 2.040		
⟨Zn–F⟩ 2.025		

TABLE V

COORDINATION OF FLUORINE IONS WITH THE DIFFERENT Zn^{2+} IN THE STRUCTURE

		Distance (Å)
Onefold	Terminal	
	F1 → Zn2	1.994
	F2 → Zn2	2.001
	F6 → Zn3	1.951
	F7 → Zn3	1.942
	⟨Zn–F[t]⟩ =	**1.980(30)**
Twofold	Bridging (*b*2)	
	F3 → Zn3	2.004
	F3 → Zn4	2.032
	F4 → Zn1	2.025
	F4 → Zn3	2.127
	F5 → Zn4	1.996
	F5 → Zn4	1.996
	F9 → Zn1	1.943
	F9 → Zn2	2.276
	⟨Zn-F[b2]⟩ =	**2.050(105)**
Threefold	Bridging (*b*3)	
	F8 → Zn2	2.031
	F8 → Zn4	2.016
	F8 → Zn4	2.016
	⟨Zn–F[b3]⟩ =	**2.021(9)**
	⟨Zn–F⟩ =	**2.035(20) in ZnF_2**

TABLE VI

VALENCE BOND ANALYSIS OF $Ba_6Zn_7F_{26}$ USING THE ZACHARIASEN LAW[a]

	Zn1	Zn2	Zn3	Zn4	Ba1	Ba2	Ba3	Σ
F1[t]	—	2 × 0.380	—	—	2 × 0.230	2 × 0.181 2 × 0.314	—	1.105
F2[t]	—	2 × 0.320	—	—	2 × 0.270	—	2 × 0.193 2 × 0.274	1.107
F3[b2b]	—	—	2 × 0.366	2 × 0.329	—	2 × 0.167	2 × 0.196	1.058
F4[b2]	4 × 0.398	—	2 × 0.228	—	2 × 0.168 2 × 0.069	2 × 0.040	2 × 0.075	0.918
F5[b2]	—	—	—	2 × 0.377	—	0.136	0.067	0.957
F6[t]	—	—	0.449	—	0.319	2 × 0.095	—	0.958
F7[t]	—	—	0.465	—	0.204	—	0.089 2 × 0.104	0.966
F8[b3b]	—	0.330	—	2 × 0.349	—	—	—	1.028
F9[b2b]	2 × 0.397	0.128	—	—	2 × 0.111	2 × 0.156	—	1.059
Σ	2.014(8)	1.96(5)	2.10(7)	2.11(5)	2.22(4)	1.89(3)	1.84(3)	—
Σ_{theor}	2	2	2	2	2	2	2	1

[a] $S = \exp(D_0 - D)/B$. D_0 represents the length of a bond in a regular polyhedron and B a fitted constant: $D_0 = 2.028(2)$ and $B = 0.2598$ for Zn–F; $D_0 = 2.685(2)$ and $B = 0.394$ for Ba–F.

[b] *b*2 and *b*3 refer to the two types of bridging fluorine (see Table V).

and the corresponding distances are in good agreement with previous data (*10, 11*) and the sum of ionic radii (*12*). However, the situation of the Zn2–F9 bond (2.276 Å) seems anomalous. A valence bond analysis (*9, 14*), which appears in Table VI, shows that the bond strength of F9 is approximately three times lower than the others around Zn2 and explains that a long Zn2–F9 distance is normal, the bonding possibilities of Zn2 being quite "saturated" by the fluorine F1, F2, and F8. The coordination of Zn2 is then better described by (5 + 1) than 6. This fact is correlated to the short F1–F2 distances. Zn^{2+} cannot be inserted in the square plane of F1 and F2 ions (the permitted radius is only 0.67 Å compared to $r_{Zn}2+ = 0.74$ Å). It shifts out of the plane; the presence of Ba1 and Ba2 ions near F9 and F1 obliges Zn^{2+}, for electrostatic repulsion reasons, to be displaced toward F8. The Zn2–F9 distance is then increased.

The ZnF_6 octahedra share edges and corners to ensure a three-dimensional network. In the (002) plane, octahedra of Zn4 ions (shaded in Fig. 1) form infinite rutile chains parallel to the **b** axis of the cell, the dimension of which corresponds to two edge-sharing octahedra. Zn2 and Zn3 octahedra share some of their corners with Zn1 and Zn4 octahedra in a rather complicated way. Two different types of description render the analysis of their connection easier: the first uses connected layers, the second starts from defective rutile blocks. In each case, it will be necessary to compare the networks of $Ba_6M_7F_{26}$ (M/Ba = 1.167) and $Ba_2M_3F_{10}$ (M/Ba = 1.50). Then, a possible mechanism of structural evolution in the M/Ba ≥ 1 part of the binary diagram BaF_2–MF_2 will be proposed, the limit of this evolution being the rutile structure.

1. Connected Layers

The connection of Zn1, Zn3, and Zn4 octahedra in the (200) plane builds layers which appear in Fig. 2a. In these layers, two consecutive rutile chains (Zn4 octahedra) are separated by a complete planar perovskite block, i.e., three rows (Zn3–Zn1–Zn3) of corner-sharing octahedra. Two consecutive layers are shifted of *b*/2

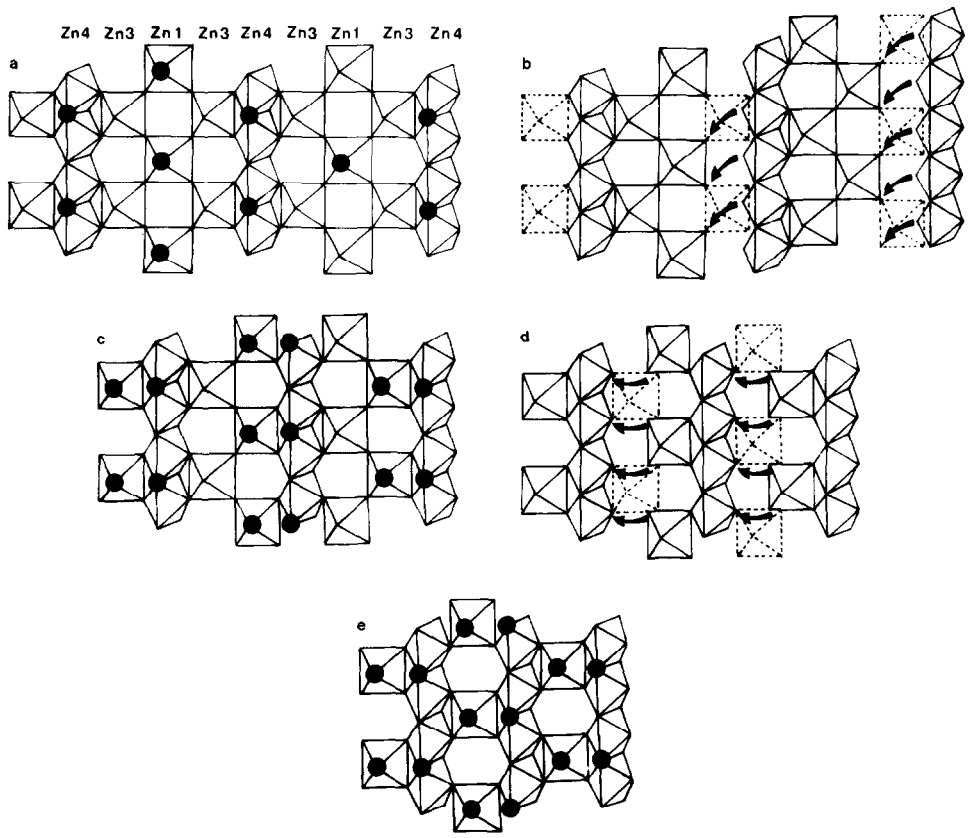

FIG. 2. (a) Perspective view of the layer in the (200) plane. Full circles indicate the fluorine atoms shared with the Zn2 isolated octahedra which ensure the connection between two layers. For this symbolism, there is no correlation with those of Fig. 1. (b) Proposed intermediate step for the transformation from $Ba_6M_7F_{26}$ to $Ba_2Ni_3F_{10}$. (c) Perspective view of the layer in the (002) plane of the $Ba_2Ni_3F_{10}$ structure. (d) Extrapolated intermediate step in the condensation of $Ba_2Ni_3F_{10}$. (e) Perspective view of the layer of a possible structure corresponding to $Ba_2M_5F_{14}$ formulation.

and linked by isolated Zn2 octahedra. This last octahedron shares the F8 ion with the rutile chain of one layer, and F9 with the medium row Zn1 of the perovskite block of the other layer (owing to the *b*/2 shift mentioned above). These layers correspond to the main faces of the platelet.

A similar situation exists in the previously described (*5*) $Ba_2Ni_3F_{10}$ (Fig. 2c), but only two rows of corner-sharing octahedra separate two rutile chains. This corresponds to the elimination of one Zn3 row in the $Ba_6Zn_7F_{26}$ structure and to a correlated shift of the rutile chain according to the scheme of Fig. 2b. This figure also explains the change of the nature of the layer bridging units. They were single Zn2 octahedra in $Ba_6Zn_7F_{26}$ and became isolated bioctahedra in $Ba_2Ni_3F_{10}$. Such a procedure corresponds to a condensation mechanism. If it is extrapolated, (Fig. 2d), it may be assumed that the following step, unknown in the diagram at the present time, would lead to the structure which appears in Fig. 2e. The corresponding formula would be $Ba_2M_5F_{14}$. In this hypothesis, it is noteworthy that the bridging isolated bioctahedra would be connected to each other in order

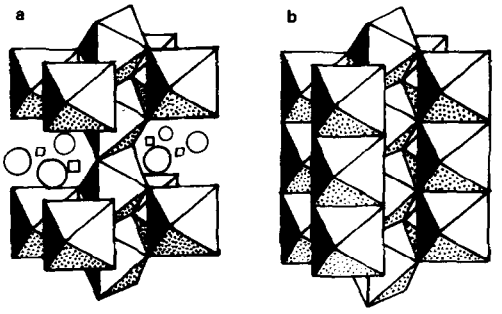

FIG. 3. (a) Perspective view of the deficient rutile blocks in $Ba_6Zn_7F_{26}$. Zn vacancies are noted by open squares and Ba^{2+} ions by open circles. (b) Perspective view of the corresponding rutile structure.

to form planes identical to those which exist in the $CaTa_2O_6$ structure (*13*). However, the interstices occupied by Ba^{2+} ions would be relatively small; in other words, if such a structure does exist, it can only be with smaller alkali earth ions.

2. *Defective Rutile Blocks*

From Fig. 1, it can be seen that each Zn4 chain is surrounded by four satellite octahedra (2 Zn2 + 2 Zn3). Their projection on the (010) plane is reminiscent of the rutile structure. However, the perspective views of Fig. 3 illustrate the difference between these two units. In the rutile structure (Fig. 3b), the satellites form also chains of edge-sharing octahedra, whereas in $Ba_6Zn_7F_{26}$ (Fig. 3a), half of the 3*d* metallic sites are missing. Satellite chains of the rutile structure become a succession of filled octahedra separated by Ba^{2+} ions which roughly occupy the corresponding F^- sites in the rutile structure. In $Ba_6Zn_7F_{26}$, Zn1 octahedra ensure the connection of these blocks (Fig. 4a). In $Ba_2Ni_3F_{10}$, identical units are directly connected one to the other (Fig. 4b), owing to the condensation mechanism proposed above. The further progressive transformation into the rutile structure would occur by the replacement of Ba^{2+} by 3*d* M^{2+} ions, simultaneously with the change of terminal F^- into bridging ones.

The coordination polyhedra of Ba1, Ba2, and Ba3 can be easily described if the $(20\bar{1})$ planes of the structure are considered: barium and fluorine ions form together slightly distorted dense packing layers parallel to these planes; barium ions adopt the 12-coordination characteristic of this type of packing. In the pseudo-orthorhombic cell (Fig. 5) obtained by the matrix

$$\begin{bmatrix} a_0 \\ b_0 \\ c_0 \end{bmatrix} = \begin{bmatrix} 2 & 0 & \bar{1} \\ 0 & 1 & 0 \\ 1 & 0 & 2 \end{bmatrix} \begin{bmatrix} a_m \\ b_m \\ c_m \end{bmatrix},$$

the structure can be described in terms of dense packing with 12 layers corresponding to the sequence $A_4^{1,2}B_2^3A_2^3B_4^{1,2}C_4^{1,2}A_2^3C_2^3A_4^{1,2}$

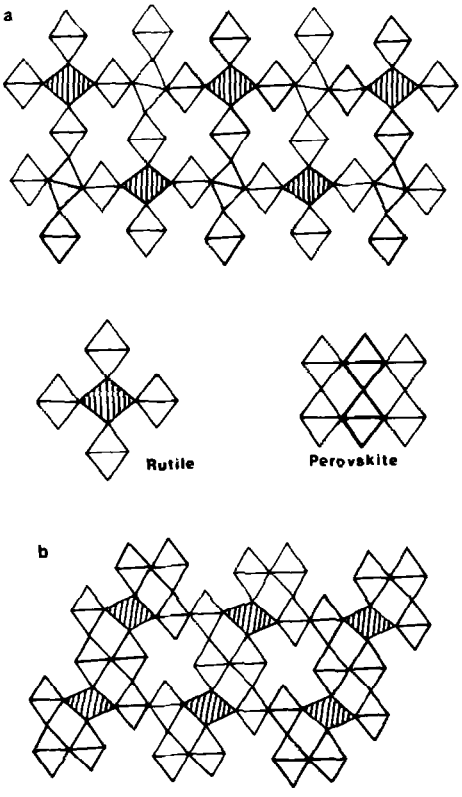

FIG. 4. Relative disposition of the defective rutile blocks in $Ba_6Zn_7F_{26}$ (a) and $Ba_2Ni_3F_{10}$ (b) projections on the (010) plane. The representation of rutile and perovskite blocks appears between (a) and (b).

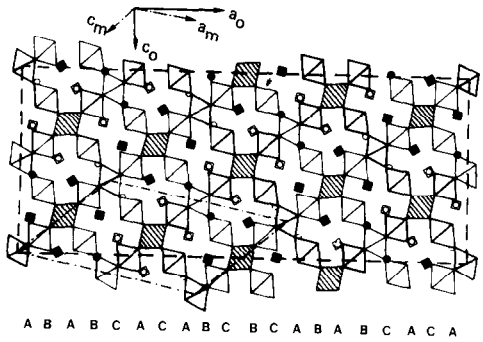

FIG. 5. Representation of $Ba_6Zn_7F_{26}$ in terms of dense packing (the first 20 layers have been represented). The symbols for Ba^{2+} ions are the same as that in Fig. 1.

$B_4^{1,2}C_2^3B_2^3C_4^{1,2}$. In this notation, the higher indices refer to the type of Ba (Ba1, Ba2, or Ba3) which is inserted in the considered layer, and the lower ones (2 or 4) to the number of barium ions in the layer. These indices correspond to the compositions Ba_2F_{14} for indice 2 and Ba_4F_{12} for indice 4 which were encountered also in $Ba_2Ni_3F_{10}$, but with a different mode of stacking. Consequently, the three (4*i*) sites of Ba^{2+} adopt a 12-coordination of the hcp type for Ba3 and of the fcc type for both Ba1 and Ba2. Keeping in mind that in rutile, the close packing of F^- is exclusively of the hcp type, it is normal to ascertain the increase of the percentage of this type of site (33.3% in $Ba_6Zn_7F_{26}$, 50% in $Ba_2Ni_3F_{10}$, 100% in MF_2) with the *M*/Ba ratio.

In all the cases (Table VII), the average value of Ba–F distances (2.848 Å for Ba1, 2.937 Å for Ba2, 2.920 Å for Ba3, ⟨Ba–F⟩ = 2.901 Å) is very close to the sum of ionic radii of $^{XII}Ba^{2+}$ (1.61 Å) and $^{II}F^-$ (1.285 Å) (*12*). F–F distances being always longer than $2r_{F^-}$, it can be thought that the insertion of Ba^{2+} ions in the fluorine layers is responsible of this observed increase of distance between F^- ions, and consequently of the decrease of the packing ratio τ from 0.74 ideal value to 0.608 when only Ba^{2+} and F^- are considered ($\tau = 0.63$ when Zn^{2+} are included).

TABLE VII

INTERATOMIC DISTANCES (Å) IN THE COORDINATION POLYHEDRA OF Ba^{2+}

Polyhedra of Ba1	
Ba1–F6:	2.589(12)
Ba1–F2:	2 × 2.655(6)
Ba1–F1:	2 × 2.718(6)
Ba1–F7:	2.765(4)
Ba1–F4:	2 × 2.841(10)
Ba1–F9:	2 × 3.004(2)
Ba1–F4:	2 × 3.194(11)
⟨Ba1–F⟩	2.848
Polyhedra of Ba2	
Ba2–F1:	2 × 2.595(6)
Ba2–F1:	2 × 2.811(6)
Ba2–F3:	2 × 2.843(7)
Ba2–F9:	2.870(12)
Ba2–F5:	2.924(9)
Ba2–F6:	2 × 3.066(3)
Ba2–F4:	2 × 3.412(10)
⟨Ba2–F⟩	2.937
Polyhedra of Ba3	
Ba3–F2:	2 × 2.649(6)
Ba3–F3:	2 × 2.781(7)
Ba3–F2:	2 × 2.786(7)
Ba3–F7:	2 × 3.030(2)
Ba3–F7:	3.090 (2)
Ba3–F4:	2 × 3.160(12)
Ba3–F5:	3.201(9)
⟨Ba3–F⟩	2.920
⟨Ba–F⟩	2.901

Conclusion

This study, and the previously described $Ba_2Ni_3F_{10}$ structure have begun to show that, in the binary diagrams $(1 - x)BaF_2$, xMF_2, the structural evolution in the $x > 0.5$ region may be described by a condensation mechanism for $0.714 \geq x > 0.5$. It could explain the transformation of structures deriving from the perovskite to the rutile structure. At the present time, the validity of the mechanism is studied for

higher values of x, particularly in $Ba_2Cu_7F_{18}$ single crystals.

Acknowledgments

The authors are grateful to Dr. P. Chevallier and Pr. Rouxel (University of Nantes) for providing them with all facilities in data collection, to Dr. J. Pannetier for helpful discussions during the bond valence analysis, and to Pr. R. De Pape for his interest.

References

1. M. Samouël, *Rev. Chim. Min.* **8,** 533 (1971).
2. E. T. Keves, S. C. Abrahams, and J. L. Bernstein, *J. Chem. Phys.* **51**(11), 4928 (1969).
3. H. G. Von Schnering, B. Kolloch, and A. Kolodziejczyk, *Angew. Chem.* **83**(12), 440 (1971).
4. H. G. Von Schnering, *Z. Anorg. Allg. Chem.* **353,** 13 (1967).
5. M. Leblanc, G. Ferey, and R. De Pape, *J. Solid State Chem.* **33,** 317 (1980).
6. G. Ferey, M. Leblanc, R. De Pape, M. Passaret, and M. Bothorel-Razazzi, *J. Cryst. Growth* **29,** 209 (1975); M. Leblanc, G. Ferey, and R. De Pape, *Mater. Res. Bull.* **19,** 1581 (1984).
7. G. M. Sheldrick, "SHELX: A Program for Crystal Structure Determination," Cambridge Univ. Press, London/New York (1976).
8. "International Tables for X-Ray Crystallography," Vol. IV, Kynoch Press, Birmingham, 1974.
9. G. Ferey, M. Leblanc, A. de Kozak, M. Samouël, and J. Pannetier, *J. Solid State Chem.* **56,** 288 (1985).
10. E. Herdtweck and D. Babel, *Z. Kristallogr.* **153,** 189 (1980).
11. H. Holler and D. Babel, *Z. Anorg. Allg. Chem.* **491,** 137 (1982).
12. R. Shannon, *Acta Crystallogr. A* **32,** 751 (1976).
13. L. Jahnberg, *Acta Chem. Scand.* **71,** 2548 (1963).
14. J. Pannetier, submitted for publication.